



Published in final edited form as:

Science. 2016 September 2; 353(6303): 1037–1040. doi:10.1126/science.aaf5206.

De novo synaptogenesis induced by GABA in the developing mouse cortex

Won Chan Oh¹, Stefano Lutz², Pablo E. Castillo², and Hyung-Bae Kwon^{1,3,*}

¹Max Planck Florida Institute for Neuroscience (MPFI), Jupiter, FL 33458, USA

²Dominick P. Purpura Department of Neuroscience, Albert Einstein College of Medicine, Bronx, NY 10461, USA

³Max Planck Institute of Neurobiology, Martinsried 82152, Germany

Abstract

Dendrites of cortical pyramidal neurons contain intermingled excitatory and inhibitory synapses. We studied the local mechanisms that regulate the formation and distribution of synapses. We found that local γ -aminobutyric acid (GABA) release on dendrites of mouse cortical layer 2/3 pyramidal neurons could induce gephyrin puncta and dendritic spine formation via GABA type A receptor activation and voltage-gated calcium channels during early postnatal development. Furthermore, the newly formed inhibitory and excitatory synaptic structures rapidly gained functions. Bidirectional manipulation of GABA release from somatostatin-positive interneurons increased and decreased the number of gephyrin puncta and dendritic spines, respectively. These results highlight a noncanonical function of GABA as a local synaptogenic element shaping the early establishment of neuronal circuitry in mouse cortex.

The spatial arrangement of synapses determines the functional consequences of excitation and inhibition for synaptic integration, action potential generation, and repetitive activity (1–5). The initial processes of synapse formation are regulated by genetically programmed intrinsic mechanisms; later, synapses are further shaped by neuronal activity (6). Recently, a fine-scale optical approach using two-photon laser scanning microscopy and two-photon laser photoactivation revealed the processes of individual excitatory synapse formation in real time and the underlying signaling pathways in various brain regions such as the neocortex, hippocampus, and basal ganglia (7–9). However, the spatiotemporal mechanisms that govern activity-dependent de novo inhibitory synapse formation in a developing circuit

*Corresponding author. hyungbae.kwon@mpfi.org.

Supplementary materials contain additional data.

Author contributions: W.C.O. and H.-B.K. conceived and designed the study; W.C.O. performed and analyzed all experiments except perforated patch-clamp recordings, which were performed and analyzed by S.L. and P.E.C.; W.C.O. prepared the figures; W.C.O. and H.-B.K. wrote the manuscript; and all authors revised the manuscript.

SUPPLEMENTARY MATERIALS

www.sciencemag.org/content/353/6303/1037/suppl/DC1

Materials and Methods

Figs. S1 to S19

Movies S1 and S2

References (30–36)

remain poorly understood. Here, we used two-photon GABA photolysis to deliver spatiotemporally controlled patterns of GABA release in mouse dendrites and monitored how GABA release influences synapse formation. These activity-induced processes were visualized as gephyrin puncta and dendritic spines, which are inhibitory and excitatory synapse markers, respectively (fig. S1) (10, 11).

We first examined the total number of gephyrin puncta along the apical and basal dendrites in organotypic slice cultures during normal development. Both gephyrin puncta and dendritic spines rapidly increased between EP6–8 and EP10–12 [EP (equivalent postnatal) day = postnatal day at slice culturing + days in vitro] (fig. S2), and these changes were not affected by Teal fluorescent protein fused to gephyrin (Teal-gephyrin) expression (fig. S3). A similar timeline of gephyrin puncta and dendritic spine formation was observed in vivo (fig. S4). These data indicate that the synapse-forming machinery operates efficiently in our experimental system. On the basis of these results, we focused on oblique dendrites localized $>70\ \mu\text{m}$ away from the soma at ages EP6 to EP8 for the following synaptogenesis experiments.

Because the timing and location of GABA release can be controlled with high spatial and temporal resolution (fig. S5) (12), we examined how local GABA release influences synaptogenesis. Repetitive GABA release [high-frequency uncaging (HFU); 60 times at 10 Hz, duration 2 ms] effectively induced the formation of gephyrin clusters, with a success rate of ~48% (Fig. 1, A and B). This finding suggests that GABA is sufficient to drive inhibitory synapse formation, analogous to glutamate-induced spinogenesis (9). In addition, we found that GABA HFU triggered dendritic spine formation (Fig. 1, A and B). To resolve whether both GABA and glutamate trigger common signaling mechanisms to generate gephyrin clusters and dendritic spines, we next performed glutamate uncaging. Unlike GABA uncaging, glutamate HFU led to spine formation but not to gephyrin clustering (Fig. 1, A and B). These results demonstrate that there is a segregated downstream mechanism that is selectively activated by GABA but not by glutamate for gephyrin clustering, suggesting the input specificity of de novo inhibitory synapse formation. To determine whether the same phenomenon could occur in vivo, we performed GABA uncaging on layer 2/3 pyramidal neurons in vivo (13). Similar to slice cultures, both gephyrin puncta and dendritic spines were induced by in vivo GABA uncaging (Fig. 1, A and C). Neither mock stimulation nor uncaging of a similar caged compound, NPEC-caged-D-AP5 (fig. S6), led to successful induction (fig. S7). When we performed the same experiments in older slices (EP14 to EP18), success rates of both gephyrin clustering and spinogenesis were reduced, but not in younger slices (EP3 or EP4) (Fig. 1B). The induction was spatially precise (Fig. 1D). However, expression mechanisms differed (Fig. 1E). Most gephyrin puncta and spines formed during the initial 5-min period after GABA HFU were stable and likely to become fully mature (Fig. 1, F and G).

To investigate whether GABA acts as an excitatory signal and triggers Ca^{2+} influx during early development (9, 14), we examined the chloride reversal potential (E_{Cl}) at P6 to P7, P11 to P14, and P18 to P24 by means of perforated patch-clamp recording. E_{Cl} was $-46\ \text{mV}$ in young neurons and $-66\ \text{mV}$ in mature neurons (Fig. 2, A and B). We found a similar E_{Cl} by single-channel recording (fig. S8). Furthermore, layer 2/3 neurons were depolarized by

GABA uncaging in cell-attached current clamp mode, and this depolarization was prevented by the chloride cotransporter (NKCC1) inhibitor bumetanide (fig. S9). GABA uncaging was sufficient to trigger Ca^{2+} influx in young neurons in a GABA_A-sensitive manner (Fig. 2, C and D). Thus, GABA, which normally acts as an inhibitory neurotransmitter in the mature brain, can initiate excitatory signaling cascades for synaptogenesis in the developing cortex.

GABA signals via ionotropic and metabotropic receptors (15). We tested the involvement of these two receptor types. GABA type A receptor (GABA_AR) blockade by GABA_A significantly reduced gephyrin clustering (Fig. 2E), whereas GABA type B receptor blockade did not alter gephyrin puncta formation (Fig. 2E), although CGP55845 reversed the baclofen-mediated reduction of cell firing (fig. S10). Given that GABA depolarizes young neurons and triggers formation of gephyrin puncta, we examined the involvement of voltage-dependent calcium channels (VDCCs). L-type VDCCs promote gephyrin and glycine receptor clustering (16) and can be activated through the Cav1.3 subunit at a hyperpolarized potential (~ -55 mV) (17). Blockade of L-type VDCCs by nifedipine did not affect gephyrin clustering but did cause dispersal of gephyrin puncta (Fig. 2E). Blockade of T-type VDCCs (low voltage-activated Ca^{2+} channels) by mibefradil, which is also a partial antagonist of L-type VDCCs, reduced GABA-induced gephyrin clustering (Fig. 2E). Spine formation by GABA uncaging was inhibited by GABA_A, nifedipine, and mibefradil (Fig. 2F). Blockade of the depolarizing action of GABA by bumetanide reduced the success rate of both gephyrin clustering and spinogenesis. Lower-frequency GABA uncaging (LFU; 1 Hz) also reduced the success rate (Fig. 2, E and F). Thus, gephyrin puncta and dendritic spine formation induced by GABA are triggered by GABA_AR activation followed by Ca^{2+} influx through L- and T-type VDCCs. Neither gephyrin clustering nor spine formation were induced by GABA uncaging in a Ca^{2+} -free artificial cerebrospinal fluid (Fig. 2, E and F).

Structural changes of newly formed spines are associated with adaptive functional changes in cortical circuits (9, 18–20), but whether gephyrin clusters can lead to functional inhibitory synapse formation is unknown. To address this question, we measured uncaging-evoked inhibitory postsynaptic currents (uIPSCs) from newly formed gephyrin puncta. When GABA HFU was delivered at the target spot in whole-cell clamp mode (fig. S11), new gephyrin puncta formed rapidly and the amplitudes of uIPSCs subsequently increased at the target location but not at a neighboring control location (Fig. 3, A to D, and fig. S12). These data imply that functional GABA_ARs are rapidly recruited to newly formed gephyrin clusters (Fig. 3, E and F). We also found that newly formed dendritic spines became functional, as indicated by glutamate uncaging-evoked AMPA receptor (AMPA)-mediated excitatory postsynaptic currents (uEPSCs) (Fig. 3, G and H). Thus, newly formed gephyrin clusters and dendritic spines gain functions by recruiting functional receptors.

To determine whether endogenous GABAergic synaptic activity also promotes both inhibitory and excitatory synaptogenesis, we used optogenetics to activate cortical interneurons. We first verified the efficacy of viral infection during early development (fig. S13 and movies S1 and S2) (21). We infected adeno-associated virus (AAV)-*dflox*. hChR2 (H134R)-mCherry after culturing cortical slices from somatostatin (SOM)-Cre mice (fig. S14); 3 to 5 days after viral infection, we delivered three rounds of blue light illumination (fig. S14). Photostimulation of ChR2-transfected SOM interneurons caused rapid formation

of new gephyrin puncta and dendritic spines in young neurons, which was blocked by GABA_Azine; the same stimulation did not make induction in old slices (Fig. 4, A and B). To examine the proximity between presynaptic boutons and new gephyrin clusters or dendritic spines, we visualized both presynaptic SOM and postsynaptic pyramidal neurons (Fig. 4C) and found that the majority of gephyrin puncta and dendritic spines were formed close (<2 μm) to the axonal boutons of SOM interneurons (Fig. 4D). Thus, GABA uncaging–induced synaptogenesis is triggered by the same mechanisms as synaptic GABA release under physiological conditions.

We next abolished GABA release by injecting AAV-containing tetanus toxin light chain (TeTxLC) inverted in a flip-excision (FLEX) cassette into EP3 culture from SOM-Cre mice (22). We confirmed that TeTxLC on its own prevented vesicle release (fig. S15) and did not affect synapse development (fig. S16). In TeTxLC-expressing SOM-Cre slices at EP11 and EP12, we found that the gephyrin puncta density in distal apical dendrites of layer 2/3 pyramidal neurons was reduced (Fig. 4, E and F, and fig. S17); this result implies that SOM-positive interneurons target distal apical dendrites of pyramidal neurons (23, 24). Spine density at apical dendrites was also reduced at EP7 (Fig. 4G), making spine numbers closer to those at EP3 or EP4 (fig. S18). Consistent with structural changes, TeTxLC expression reduced the frequency of both miniature IPSCs (mIPSCs) and miniature EPSCs (mEPSCs) in slices (Fig. 4, H and I) and in vivo (fig. S19). Thus, we suggest that early-developing GABAergic inputs from cortical interneurons control both inhibitory and excitatory circuitry during cortical development.

Our findings suggest that GABA sets the balance between inhibitory and excitatory synapses in early postnatal stages, laying the foundation for later circuit development (6, 25–27). Because the developing dendrites in our study did not have predetermined spots for inhibitory or excitatory synapses, localization of axonal boutons may be an early step in the precise formation of inhibitory and excitatory circuits (9, 28, 29). Thus, early-depolarizing GABA action appears to promote local synaptogenesis and shapes cortical circuitry during brain development.

Supplementary Material

Refer to Web version on PubMed Central for supplementary material.

Acknowledgments

We thank members of the Kwon laboratory for discussion, E. Nedivi for Teal-gephyrin, and H. Taniguchi for Flex-TeTxLC. Supported by the MPFI, a NARSAD Young Investigator grant, and NIH grants MH107460 (H.-B.K.) and MH081935 and DA017392 (P.E.C.).

REFERENCES AND NOTES

1. Branco T, Clark BA, Häusser M. *Science*. 2010; 329:1671–1675. [PubMed: 20705816]
2. Chiu CQ, et al. *Science*. 2013; 340:759–762. [PubMed: 23661763]
3. Hayama T, et al. *Nat Neurosci*. 2013; 16:1409–1416. [PubMed: 23974706]
4. Losonczy A, Magee JC. *Neuron*. 2006; 50:291–307. [PubMed: 16630839]
5. Spruston N. *Nat Rev Neurosci*. 2008; 9:206–221. [PubMed: 18270515]

6. Caroni P, Donato F, Muller D. *Nat Rev Neurosci*. 2012; 13:478–490. [PubMed: 22714019]
7. Hamilton AM, et al. *Neuron*. 2012; 74:1023–1030. [PubMed: 22726833]
8. Kozorovitskiy Y, Saunders A, Johnson CA, Lowell BB, Sabatini BL. *Nature*. 2012; 485:646–650. [PubMed: 22660328]
9. Kwon HB, Sabatini BL. *Nature*. 2011; 474:100–104. [PubMed: 21552280]
10. Chen JL, et al. *Neuron*. 2012; 74:361–373. [PubMed: 22542188]
11. van Versendaal D, et al. *Neuron*. 2012; 74:374–383. [PubMed: 22542189]
12. Matsuzaki M, Hayama T, Kasai H, Ellis-Davies GC. *Nat Chem Biol*. 2010; 6:255–257. [PubMed: 20173751]
13. Kim T, Oh WC, Choi JH, Kwon HB. *Proc Natl Acad Sci USA*. 2016; 113:E1372–E1381. [PubMed: 26903616]
14. Ben-Ari Y. *Neuroscience*. 2014; 279:187–219. [PubMed: 25168736]
15. Lüscher C, Jan LY, Stoffel M, Malenka RC, Nicoll RA. *Neuron*. 1997; 19:687–695. [PubMed: 9331358]
16. Kirsch J, Betz H. *Nature*. 1998; 392:717–720. [PubMed: 9565032]
17. Hage TA, Khaliq ZM. *J Neurosci*. 2015; 35:5823–5836. [PubMed: 25855191]
18. Knott GW, Holtmaat A, Wilbrecht L, Welker E, Svoboda K. *Nat Neurosci*. 2006; 9:1117–1124. [PubMed: 16892056]
19. Nägerl UV, Köstinger G, Anderson JC, Martin KA, Bonhoeffer T. *J Neurosci*. 2007; 27:8149–8156. [PubMed: 17652605]
20. Zito K, Scheuss V, Knott G, Hill T, Svoboda K. *Neuron*. 2009; 61:247–258. [PubMed: 19186167]
21. Batista-Brito R, Machold R, Klein C, Fishell G. *Cereb Cortex*. 2008; 18:2306–2317. [PubMed: 18250082]
22. Murray AJ, et al. *Nat Neurosci*. 2011; 14:297–299. [PubMed: 21278730]
23. Chen SX, Kim AN, Peters AJ, Komiyama T. *Nat Neurosci*. 2015; 18:1109–1115. [PubMed: 26098758]
24. Cichon J, Gan WB. *Nature*. 2015; 520:180–185. [PubMed: 25822789]
25. Cane M, Maco B, Knott G, Holtmaat A. *J Neurosci*. 2014; 34:2075–2086. [PubMed: 24501349]
26. Dejanovic B, et al. *PLOS Biol*. 2014; 12:e1001908. [PubMed: 25025157]
27. Flores CE, et al. *Proc Natl Acad Sci USA*. 2015; 112:E65–E72. [PubMed: 25535349]
28. Huang ZJ. *J Physiol*. 2009; 587:1881–1888. [PubMed: 19188247]
29. Miller M, Peters A. *J Comp Neurol*. 1981; 203:555–573. [PubMed: 7035504]

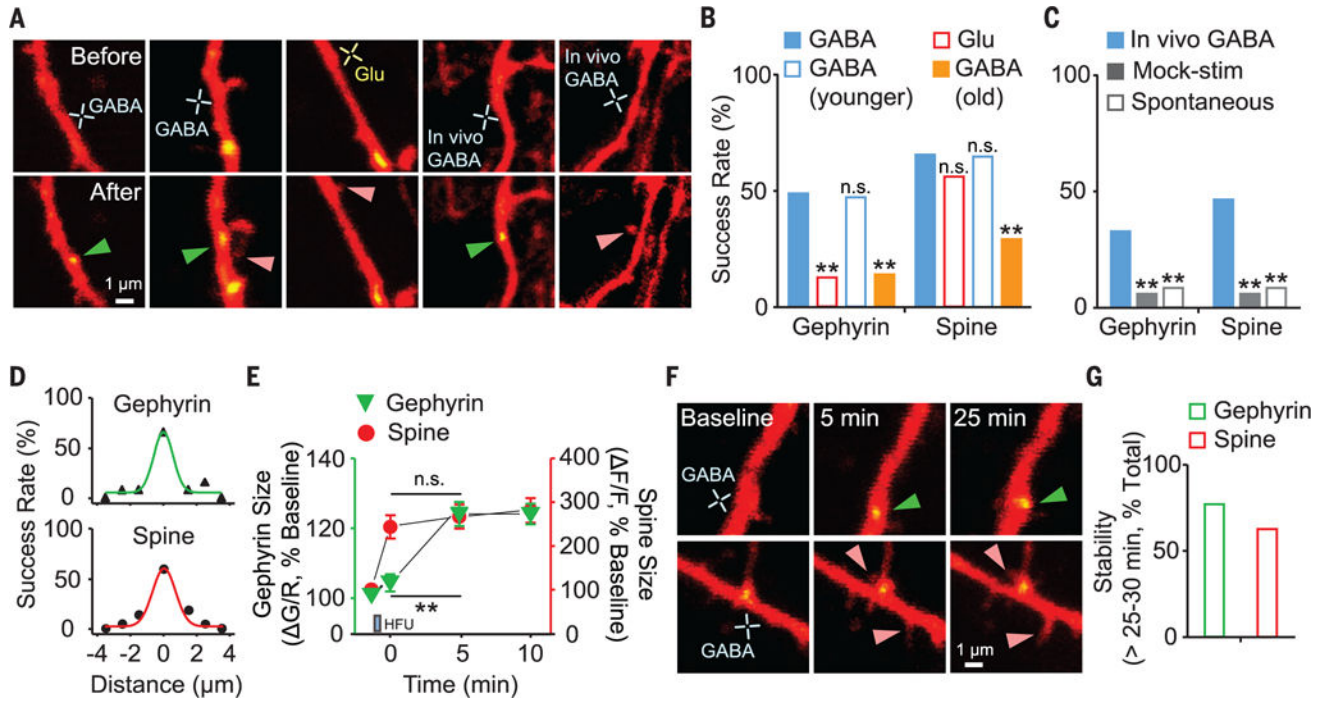


Fig. 1. GABA induces de novo formation of gephyrin puncta and dendritic spines during early development
 (A) Images of newly formed gephyrin puncta (green arrowheads) and dendritic spines (pink arrowheads) in vitro and in vivo. (B and C) Success rate of de novo gephyrin and spine formation by GABA and glutamate HFU in vitro [(B); GABA, *n* = 29 trials, 16 cells; glutamate, *n* = 24 trials, 12 cells; GABA in younger, *n* = 17 trials, 7 cells; GABA in old, *n* = 36 trials, 16 cells] and in vivo [(C); GABA, *n* = 61 trials, 55 cells, 5 mice; mock stimulation, *n* = 52 trials, 45 cells, 5 mice; spontaneous, *n* = 71 trials, 52 cells, 6 mice]. (D) Summary plots of distance-dependent de novo gephyrin and spine formation. (E) Time course for size changes of new gephyrin puncta (*n* = 18) and spines (*n* = 24). (F) Time-lapse images of GABA HFU-induced gephyrin puncta and spines. (G) Stability of newly formed gephyrin puncta (12 of 15) and dendritic spines (15 of 24). ***P* < 0.01; n.s., not significant. Error bars in (E) denote SEM.

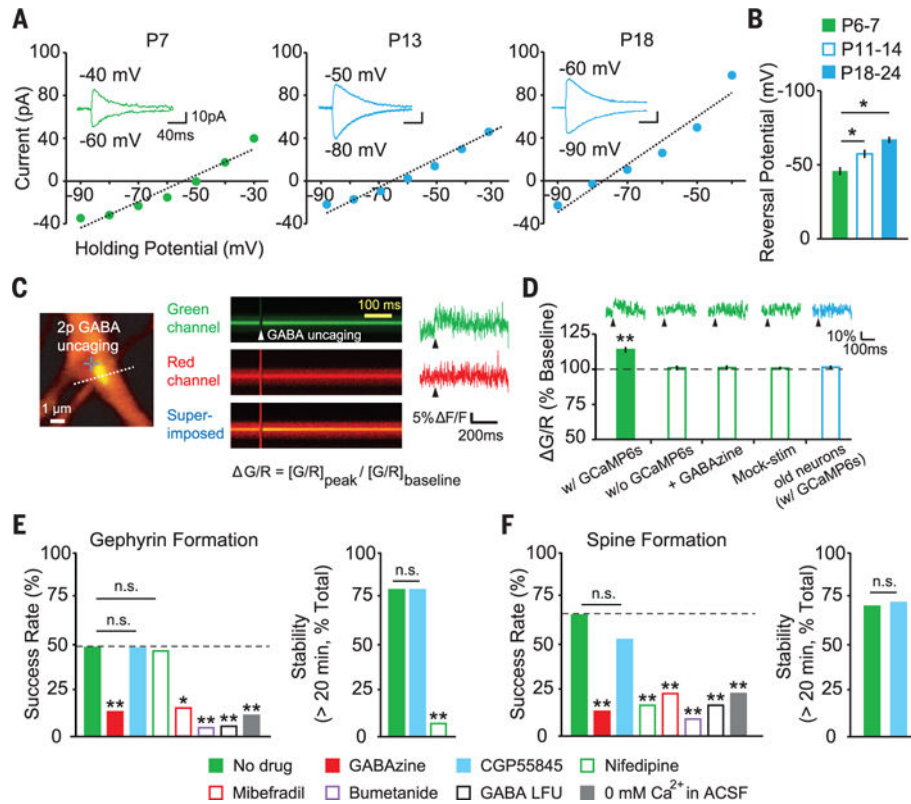


Fig. 2. Molecular mechanisms of GABA-induced de novo gephyrin puncta and dendritic spine formation

(A) Current-voltage curves measured by perforated patch-clamp recordings. (B) Summary graph of E_{Cl} at P6 to P7 (-45.9 ± 2.7 mV, $n = 5$), P11 to P14 (-57.2 ± 2.8 mV, $n = 7$), and P18 to P24 (-66.3 ± 2.1 mV, $n = 6$). (C) Image of a dendrite coexpressing GCaMP6s, tdTomato, and Teal-gephyrin. Dashed line indicates line-scan path. Green and red fluorescences were measured by line scanning before and after GABA uncaging. (D) Averaged traces and summary $\Delta G/R$ [$(G/R)_{peak} / (G/R)_{baseline}$, where G (green) is GCaMP6s fluorescence and R (red) is tdTomato fluorescence] in young (EP6 to EP8) and old (EP16 to EP18) neurons (with GCaMP6s, $n = 13$ cells; without GCaMP6s, $n = 8$; GABAzine, $n = 9$; mock stimulation, $n = 9$; old neurons, $n = 8$). (E and F) Success rate and stability of de novo gephyrin puncta and spine formation (no drug, $n = 29$ trials, 16 cells; 10 μ M GABAzine, $n = 30$ trials, 17 cells; 3 μ M CGP55845, $n = 21$ trials, 12 cells; 10 μ M nifedipine, $n = 30$ trials, 14 cells; 10 μ M mibefradil, $n = 26$ trials, 13 cells; 10 μ M bumetanide, $n = 21$ trials, 9 cells; GABA LFU, $n = 18$ trials, 8 cells, 1 Hz; 0 mM Ca^{2+} , $n = 26$ trials, 14 cells). * $P < 0.05$, ** $P < 0.01$; error bars represent SEM.

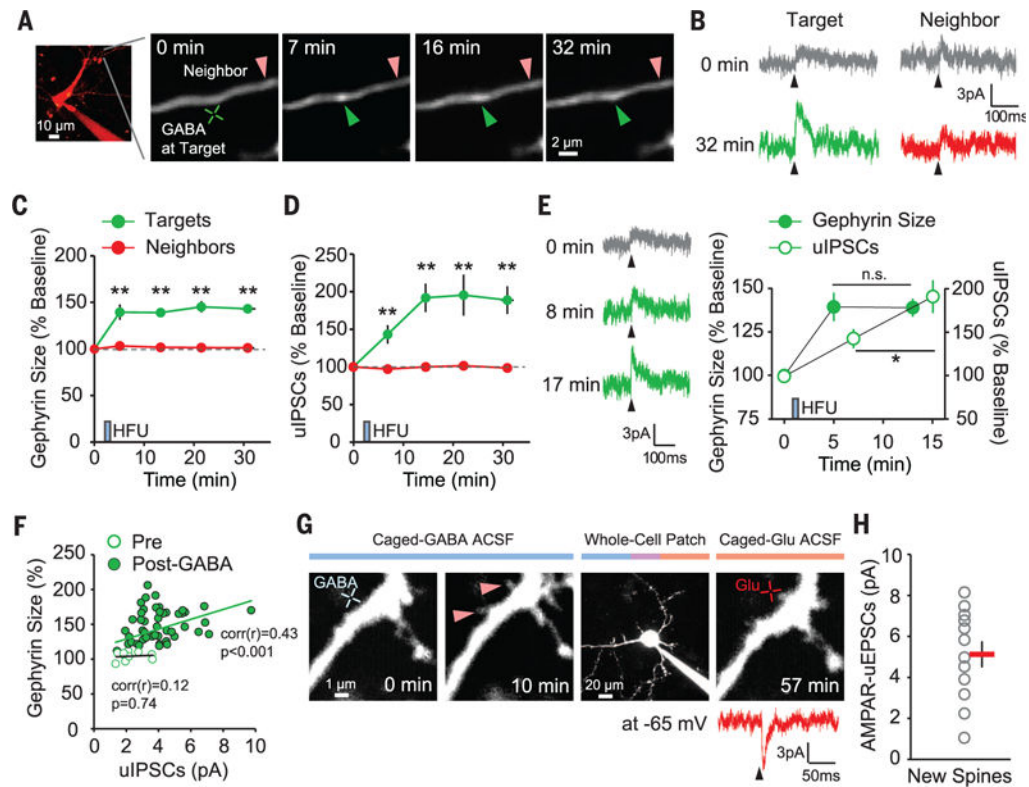


Fig. 3. Rapid accumulation of functional receptors at newly formed gephyrin puncta and dendritic spines

(**A**) Time-lapse images of a dendrite after GABA HFU. Green and red arrowheads indicate target and control spots, respectively. (**B**) uIPSC traces (average of 8 to 10 trials at 0.1 Hz, +10 mV) measured by whole-cell voltage-clamp recordings. (**C** and **D**) Time courses of the changes in gephyrin fluorescence (**C**) and uIPSC amplitudes (**D**) at targets ($n = 10$ regions) and neighbors ($n = 10$, 10 cells). (**E**) uIPSCs from a target at different time points. Time course of gephyrin fluorescence and uIPSC amplitude changes at targets. (**F**) Scatterplot between gephyrin expression levels and uIPSC amplitudes ($n = 10$ cells; up to 40 min). (**G**) Time-lapse images of a dendrite after GABA HFU (blue cross). Red arrowheads indicate new spines. uEPSCs were evoked by glutamate uncaging (red cross, 8 to 10 trials at 0.1 Hz, -65 mV) from a new spine measured by whole-cell voltage-clamp recordings. (**H**) AMPAR-mediated uEPSCs from newly formed dendritic spines ($n = 12$ spines, 5 cells). * $P < 0.05$, ** $P < 0.01$; error bars represent SEM.

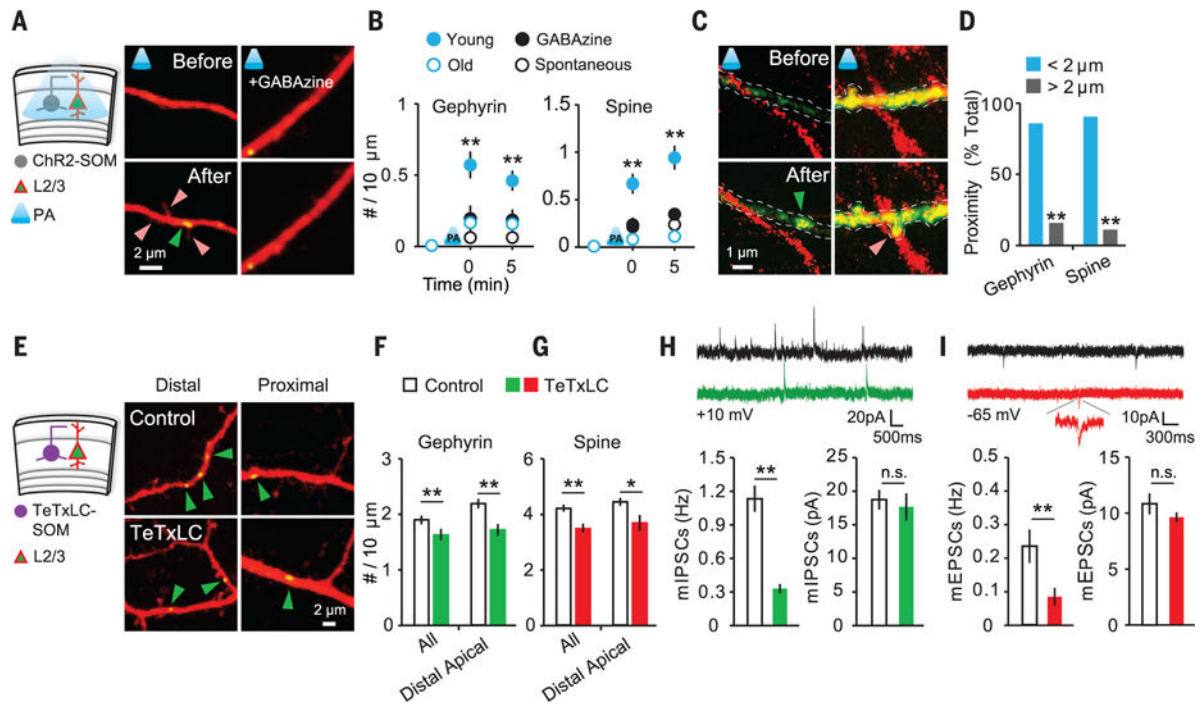


Fig. 4. GABA release from SOM interneurons is sufficient and necessary for inhibitory and excitatory synaptogenesis during early development

(A) Experimental schematic and images of newly formed gephyrin cluster (green arrowhead) and spines (red arrowheads). (B) Summary data of photoactivation-induced de novo synaptogenesis (young, $n = 23$ dendrites, 13 cells; GABAzine, $n = 22$ dendrites, 13 cells; old at EP16 to EP18, $n = 19$ dendrites, 11 cells; spontaneous, $n = 13$ dendrites, 11 cells). (C) Axons of SOM and de novo gephyrin punctum (green arrowhead) and dendritic spine (red arrowhead) imaged at 1045 nm. (D) Proximity between an axon of SOM and a new gephyrin cluster (<2 μm: 28 of 33 new puncta, 17 cells) or spine (<2 μm: 35 of 39 new spines). (E) Experimental schematic and images of dendrites in noninfected and TeTxLC-infected slices at EP12. (F and G) Quantitative analysis of gephyrin puncta density at EP11 and EP12 (control, $n = 13$ cells; TeTxLC, $n = 15$ cells) and spine density at EP7 (control, $n = 8$ cells; TeTxLC, $n = 10$ cells). (H and I) Traces of mIPSCs (H) and mEPSCs (I) measured by whole-cell patch-clamp recordings. Quantitative analyses of mIPSCs (control, $n = 11$ cells; TeTxLC, $n = 11$ cells) and mEPSCs (control, $n = 7$ cells; TeTxLC, $n = 11$ cells) are shown. * $P < 0.05$, ** $P < 0.01$; error bars represent SEM.